

Comparative Analysis of 3D Graphene–LiOH·H₂O Composites by Modification with Phytic Acid and Ascorbic Acid for Low-Grade Thermal Energy Storages

Lin Li, Shijie Li, Tao Zeng,* Lisheng Deng, Hongyu Huang,* Jun Li, Noriyuki Kobayashi, Lin Liu, and You Zhou

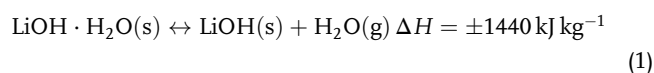
3D Graphene (3D-GF) modified with different additive concentrations (phytic acid [PA] and ascorbic acid [AA]) is developed and then combined with different LiOH contents by the hydrothermal method to obtain composite materials. It can be found that the addition of PA and AA will not destroy the carbon skeleton structure of 3D-GF. With increasing additive content, the thermal conductivities of modified 3D-GF first increase and reach their maximum values at 8 mg mL⁻¹. The modified 3D-GF with the highest thermal conductivity is selected to be combined with different LiOH contents. The addition of PA and AA can broaden the charging temperature range from 60–110 to 30–200 °C and improve the LiOH hydration rate and heat storage density. Compared with the PA-modified composite, the AA-modified composite shows smaller (about 7.6 nm) and more uniform LiOH·H₂O particles (the particles size standard deviation of 3D-GF-AA-LiOH·H₂O is 1.1503), a larger specific surface area (119 m² g⁻¹), higher heat storage density (the highest value of 2763 kJ kg⁻¹ for LiOH·H₂O, which can be about 4.2 times of pure LiOH), and less influenced by the change of LiOH content (the thermal conductivity standard deviation of 3D-GF-AA-LiOH·H₂O is 0.123).

latent,^[5,6] and thermochemical storage (TCS) systems,^[7–10] are prospective means to bridge the time and space lag between energy supply and demand.^[11] TCS, which can upgrade the stored heat at an arbitrary temperature with high heat storage densities,^[12–15] and no heat loss,^[16] is more suitable for efficient utilization of low-grade thermal energy. There are many literature that have described the adsorption process of metal salts with water,^[17–20] ammonia,^[21–25] methanol,^[26–28] or metal alloys,^[29,30] for utilizing low-grade thermal energy.

Among all the reaction systems, the inorganic hydrate lithium hydroxide monohydrate (LiOH·H₂O) due to its high energy density (1440 kJ kg⁻¹) and mild reaction process was selected as the promising candidate for low-temperature (below 373 K) heat storage.^[31] The reversible chemical reaction is as follows

1. Introduction

Low-grade energy (from ambient temperature to 523 K) such as industrial waste heat and solar energy, has the characteristics of large energy storage and wide distribution.^[1] However, the utilization of low-grade energy is prevented by its instability and the mismatch between energy supply and demand.^[2] Thermal energy storage technologies, can be divided into sensible,^[3,4]



However, the low hydration rate of LiOH as a key factor still limits the application and development of this chemical heat storage system.^[32] To solve this problem, some scholars synthesized various composite thermochemical materials (TCMs).^[33–37] Our research group also have studied the performance of LiOH·H₂O

L. Li, Dr. T. Zeng, L. Deng, Prof. H. Huang, Prof. J. Li, Dr. L. Liu
Guangzhou Institute of Energy Conversion
Chinese Academy of Sciences
Guangzhou 510640, P. R. China
E-mail: zengtao@ms.giec.ac.cn; huanghy@ms.giec.ac.cn


L. Li
University of Chinese Academy of Sciences
Beijing 100049, P. R. China

L. Li, Dr. T. Zeng, L. Deng, Prof. H. Huang, Prof. J. Li, Dr. L. Liu
Key Laboratory of Renewable Energy
Chinese Academy of Sciences
Guangzhou 510640, P. R. China

Dr. S. Li
Institute of Carbon Materials Science
Shanxi Datong University
Datong, Shanxi 037009, P. R. China

Prof. N. Kobayashi
Department of Chemical Engineering
Nagoya University
Nagoya 464-8603, Japan

Prof. Y. Zhou
National Institute of Clean-and-Low-Carbon Energy
China Energy Investment Corporation Ltd.
Beijing 102211, P.R. China

 The ORCID identification number(s) for the author(s) of this article can be found under <https://doi.org/10.1002/ente.202001086>.

DOI: 10.1002/ente.202001086

modified with hydrophilic or carbon nanoadditives. The addition of graphene oxide (GO) helps widen the range of thermal storage temperature but has little effect on the thermal conductivity.^[38] However, the addition of 3D-nickel-carbon nanotubes (3D-Ni-CNTs) has the opposite effect.^[39]

In addition to having the unique network structure,^[40–42] ultrahigh porosity, large specific surface area (about $2600 \text{ m}^2 \text{ g}^{-1}$),^[43–46] and outstanding mechanical flexibility^[47] of natural graphene, 3D graphene (3D-GF) has many other advantages according to different activators, such as high hydrophilicity,^[48–50] which was chosen as a support material for hydration reactions.^[51,52] Due to these characters, 3D-GF has been recombined with phase change materials (PCMs) such as paraffin wax to make the energy conversion and storage performances better.^[53–55] However, it is seldom used in TCS and only a small number of scholars have done research. For example, Ousaleh et al. combined MgSO_4 , MgCl_2 , and their mixture into the graphene matrix making a new hybrid TCMs for low-to-medium temperature heat storage applications and improved the cycling stability of the TCMs.^[56] Our previous study found that the addition of 3D-GF can broaden the temperature range of heat storage, but the improvement of thermal conductivity is limited.^[57] In addition, to effectively modify the hydrophilic properties of the 3D-GF surface, the $-\text{OH}$, $-\text{PO}_4$, and other functional groups can be introduced in 3D-GF production process. PA can produce a large number of active surface sites on the 3D-GF surface,^[58,59] and a large number of $-\text{PO}_4$ in PA can endow it the ability to introduce pores during carbon manufacture.^[60] AA with abundant $-\text{OH}$ can effectively improve the 3D-GF lattice and its hydrophilic properties.^[61,62] To improve the heat and mass transfer performance of the composites, this article starts from three directions: expanding the temperature range of available heat energy, minimizing the influence of LiOH ratio on the composites' thermal conductivity and increasing the reaction area of composites. LiOH was incorporated into the additive (PA or AA)-modified 3D-GF to improve the heat storage performance of LiOH and investigate the influence of additive concentration and LiOH loading content on the structure and thermochemical property of the synthesized composite material for use in the low-grade thermal energy storage system. The modified 3D-GF host matrix and modified 3D-GF-LiOH- H_2O composites are characterized by scanning electron (SEM), transmission electron micrograph (TEM), X-ray diffraction (XRD), N_2 adsorption isotherm, heat flow meter method, and thermogravimetric-differential scanning calorimetry (TG-DSC).

2. Results and Discussion

2.1. 3D-GF Morphology and Structure Characterization

In our previous studies, we determined the optimal preparation conditions of 3D-GF by hydrothermal method (reaction time 12 h, reaction temperature 180° , GO concentration 25 mg mL^{-1} , thermal conductivity $3.593 \text{ W [m}\cdot\text{K}]^{-1}$).^[57] Figure 1 shows the influence of PA and AA concentration on the thermal conductivity of 3D-GF. With the increase in the additive concentration, the thermal conductivity of 3D-GF increases first and then decreases. The thermal conductivity of 3D-GF

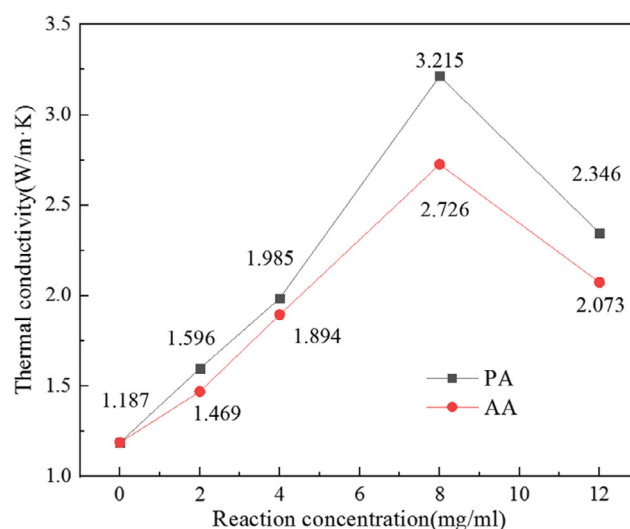


Figure 1. Thermal conductivity of 3D-GF with different additive concentrations.

reaches its maximum value when the additive concentration is 8 mg mL^{-1} . Therefore, 8 mg mL^{-1} is finally selected as the optimal concentration of additive. Both 3D-GF-PA and 3D-GF-AA show a decrease in thermal conductivity compared with pure 3D-GF. Due to the increased concentrations of PA and AA in the additive, it may disrupt the original graphene's carbon skeleton structure: the addition of PA promoted the etching of the carbon framework;^[63] the oxygen-containing groups on carbon surface actually represent a type of defects,^[62] and a possible reason for this peak broadening could be the lack of long-range order of reduced GO sheets and the presence of residual oxygen functionalities.^[61]

The phase characteristic composition of these materials is shown in Figure 2. It meets JCPDS No.41-1487 criteria and demonstrates the presence of graphite.^[64] The XRD patterns of modified 3D-GF samples are similar to that of pure 3D-GF. The diffraction peak of graphite carbon is at 25° and 43° , respectively,

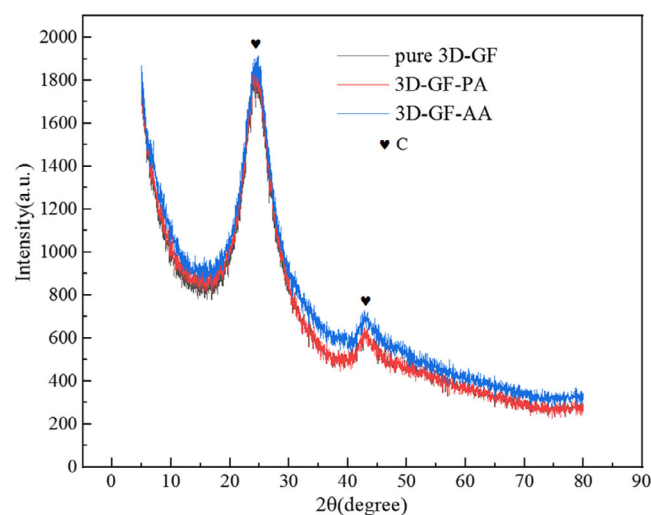


Figure 2. XRD patterns for pure 3D-GF, 3D-GF-PA, and 3D-GF-AA.

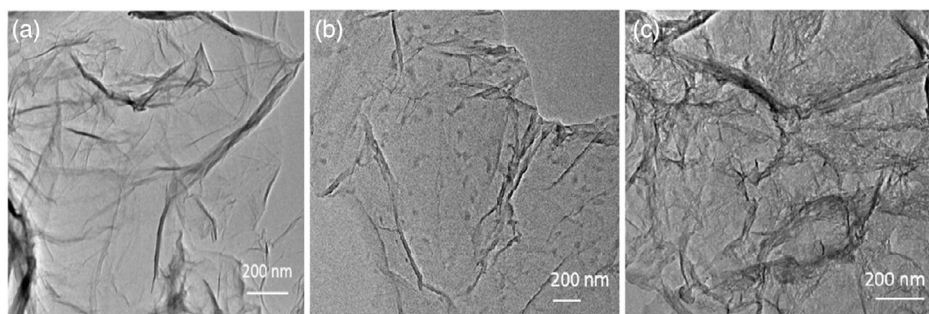


Figure 3. TEM images for: a) pure 3D-GF, b) 3D-GF-PA, and c) 3D-GF-AA.

corresponding to the (002) and (100) crystal planes of graphite structure.^[65] The intensity of 3D-GF-PA is slightly lower than that of 3D-GF and 3D-GF-AA, which may be due to the reduction of graphene sheet size after the hydrothermal reaction. The overall trend and intensity data of these three groups are consistent, indicating that the main carbon skeleton structure of the modified 3D-GF has not been destroyed.

As shown in **Figure 3b**, the 3D-GF-PA sample has a transparent sheet structure, and numerous dots can be clearly observed in the center and edge of the sheet, which is different from the result of the pure 3D-GF. It indicates that the surface of the 3D-GF sheet was modified by the $-\text{PO}_4$ group, resulting in changes in the lamellar structure of some regions during the hydrothermal reaction process^[63] and the $-\text{PO}_4$ group is relatively large, so it forms lots of shadows. **Figure 3c** shows that the sheet of 3D-GF-AA is thicker than that of 3D-GF-PA. In addition, due to the higher reduction degree of graphene caused by AA, a large number of graphene sheets stacked on each other can be observed in some parts of the sample.^[66]

2.2. 3D-GF-LiOH·H₂O morphology and structure characterization

Figure 4b,c shows XRD patterns of 3D-GF and 3D-GF-LiOH·H₂O composites modified by PA and AA, respectively. Diffraction peaks at around 15°, 20°, 30°, 32.19°, 34.84°, 38.83°, 50°, 56°, and 60° are attributed to LiOH·H₂O, and diffraction peaks at 25° and 43° belong to graphite carbon in 3D-GF.^[64,65] Compared with the unmodified 3D-GF-LiOH·H₂O composites in **Figure 4a**, the diffraction intensities of graphite carbon in the modified composites are enhanced, which indicates that the modification by PA and AA are beneficial to the formation of 3D carbon skeleton structure on graphene. Comparing **Figure 4b,c**, it is found that the diffraction intensity at 15° (LiOH·H₂O) and 25° (graphite carbon) are greater in **Figure 4c**. Therefore, AA modification is more conducive to forming the 3D carbon skeleton structure on graphene and the increase in LiOH·H₂O loading content in 3D-GF. It may be due to that AA molecule is highly water soluble (the solubility is 333 g L⁻¹ at 20 °C),^[67] and easily access the carbon surface, improving the reaction efficiency.^[62]

As shown in **Figure 5** (1-a to 1-f), a large number of particles with a larger diameter of about 100–200 nm and particles with a smaller diameter of about 10–20 nm can be observed on the 3D-GF surface. These diagrams correspond to the TEM diagrams

(**Figure 3a,b**) of 3D-GF-PA and 3D-GF-AA. Compared with 3D-GF-PA-LiOH·H₂O, it can be observed that the particles on the surface of 3D-GF-AA-LiOH·H₂O are smaller and more uniform, and no 100 nm grade particles exist, as shown in **Figure 5** (2-a to 2-f). Therefore, it can be inferred that the larger particles in 3D-GF-PA-LiOH·H₂O are PA particles, and AA is more conducive to the dispersion of LiOH·H₂O on the surface of the 3D-GF.

According to **Figure 6** (1-a to 1-f) and **7**, it is shown that the LiOH·H₂O particles are successfully dispersed on the surface of 3D-GF, and the particle size of LiOH·H₂O increases with increasing LiOH content (from 7.6 nm at 37% to 13.4 nm at 70%). Our previous study showed that 10–20 nm particle could not be detected until the LiOH content higher than 60%; however, in the PA-modified case, 10–20 nm and 100–200 nm particles can be discovered on the surface in all LiOH contents (37–70%). Therefore, we can infer that the particles with a size of 100–200 nm are PA, whereas the particles with a diameter of 10–20 nm are LiOH·H₂O. Also, the LiOH·H₂O particle sizes in the 3D-GF-PA-LiOH·H₂O composites are slightly larger than those of the unmodified and AA-modified ones, that may associate with the introduction of $-\text{PO}_4$ groups on the surface of 3D-GF. The nanosized LiOH·H₂O particles can also be identified on 3D-GF-AA-LiOH·H₂O, as shown in **Figure 6** (2-a to 2-f), and have the same relationship between the particle size of LiOH·H₂O and the LiOH content as in 3D-GF-PA-LiOH·H₂O, but show a more gently upward trend. The particles size standard deviation of 3D-GF-AA-LiOH·H₂O is 1.15036 which is less than that of LiOH·H₂O(3.0435) and 3D-GF-PA-LiOH·H₂O(2.5744). Consequently, it can be concluded that the AA can effectively induce the formation and dispersion of nanosized LiOH·H₂O particles in 3D-GF, and the particle size is more uniform and less affected by the LiOH content compared with PA.

The Brunauer-Emmett-Teller (BET) results show that the specific surface area of the 3D-GF-AA-LiOH·H₂O is 7.9 times that of the pure LiOH·H₂O and reaches its maximal value of 119 m² g⁻¹. **Figure 8** shows that the pore size distribution of the two types of modified composites are consistent with that of the unmodified 3D-GF-LiOH·H₂O composites, demonstrating that the modification of 3D-GF by the two additives have no effect on the pore size distribution. According to the BET method, the pore size distribution and pore structure type of porous carbon can be obtained, and the maximum pore size distribution is around 4 nm. This indicates that all samples are mainly composed of a considerable number of small-scale mesopores (ranging from 2 to 5 nm). The

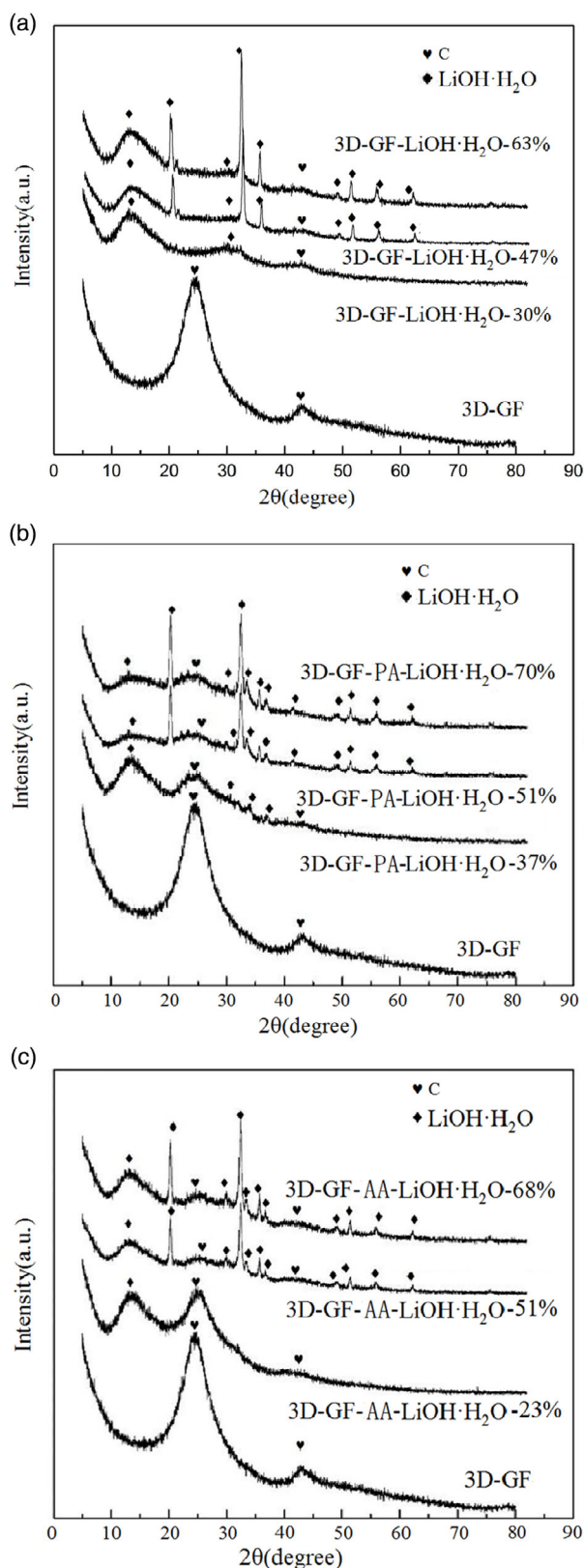


Figure 4. XRD patterns of: a) 3D-GF and unmodified 3D-GF-LiOH·H₂O composites; b) 3D-GF and 3D-GF-PA-LiOH·H₂O composites; c) 3D-GF and 3D-GF-AA-LiOH·H₂O composites.

specific surface area of 3D-GF-AA-LiOH·H₂O (119 m² g⁻¹) is higher than that of 3D-GF-PA-LiOH·H₂O (68 m² g⁻¹) and unmodified 3D-GF-AA-LiOH·H₂O (119 m² g⁻¹) is higher than that of 3D-GF-PA-LiOH·H₂O (68 m² g⁻¹) and unmodified 3D-GF-LiOH·H₂O composites (100 m² g⁻¹) in Table 1. According to the SEM images, the particle size of PA is larger than that of AA, so the specific surface area of 3D-GF-AA-LiOH·H₂O is larger for the composites with the same quality. In addition, it is evident that the pore size distribution of modified composites, regardless of the LiOH content and the additive type, is lower than that of the pure LiOH·H₂O (Figure 8a).

The thermal storage performance and reaction mechanism of composite materials are studied by TG-DSC curve. Figure 9a,b,d, e-g shows the TG-DSC measurement results of pure LiOH·H₂O, 3D-GF-PA-LiOH·H₂O, and 3D-GF-AA-LiOH·H₂O after 1 h hydration, respectively. The conversion of LiOH (conversion_{LiOH}) is calculated according to the following equation

$$\text{conversion}_{\text{LiOH}} = \frac{(w_{\text{loss}} \times \frac{23.94}{18})}{(1 - w_{\text{loss}}) \times z} \times 100\% \quad (2)$$

where w_{loss} is the weight loss rate and z is the weight percentage of LiOH in the composites.

Due to the slow hydration rate of pure LiOH, only 28.21% LiOH is hydrated after 1 h, and its heat storage density is only about 661 kJ kg⁻¹ (Figure 10). Compared with the pure LiOH, the conversion of LiOH in composites can reach about 81.34% (3D-GF-PA-LiOH·H₂O-70%) and 79.88% (3D-GF-AA-LiOH·H₂O-68%) after 1 h, so the addition of PA and AA is beneficial to the increase in LiOH hydration rate. By changing the LiOH content, the heat storage density of composites can reach 627 kJ kg⁻¹ (37%), 790 kJ kg⁻¹ (51%), and 1043 kJ kg⁻¹ (70%), respectively, in 3D-GF-PA-LiOH·H₂O, and the highest heat storage density of LiOH·H₂O monomer can be increased to 1695 kJ kg⁻¹ (3D-GF-PA-LiOH·H₂O-37%), which is 2.6 times of pure LiOH·H₂O. Compared with the highest heat storage density of LiOH·H₂O monomer in unmodified 3D-GF-LiOH·H₂O (1830 kJ kg⁻¹), its heat storage density decreases by 7.4%. The reason is that PA reduces the composites' specific surface area and forms a certain cover on the LiOH·H₂O particles, which hinders the hydration reaction and makes the composites' heat storage density decrease slightly.

In the case of 3D-GF-AA-LiOH·H₂O, the heat storage density of composites can reach 635 kJ kg⁻¹ (23%), 1100 kJ kg⁻¹ (51%), and 1300 kJ kg⁻¹ (68%), respectively, and the highest heat storage density of LiOH·H₂O monomer can be increased to 2763 kJ kg⁻¹ (3D-GF-AA-LiOH·H₂O-23%), which is 4.2 times of pure LiOH·H₂O. Compared with the highest thermal storage density of LiOH·H₂O monomer in unmodified 3D-GF-LiOH·H₂O (1830 kJ kg⁻¹), the thermal storage density of 3D-GF-AA-LiOH·H₂O is increased by nearly 50%. The reasons for the high heat storage density of the 3D-GF-AA-LiOH·H₂O are threefold. First, the introduction of AA makes a large number of hydrophilic groups such as hydroxyl group, carbonyl group, and carboxyl group on the surface of 3D-GF, which provides an excellent hydrophilic reaction interface for the hydration reaction of LiOH·H₂O, and enhances the adsorption of water molecules on the material. Furthermore, the addition of AA increases the composites' specific surface area, enhances the dispersity of

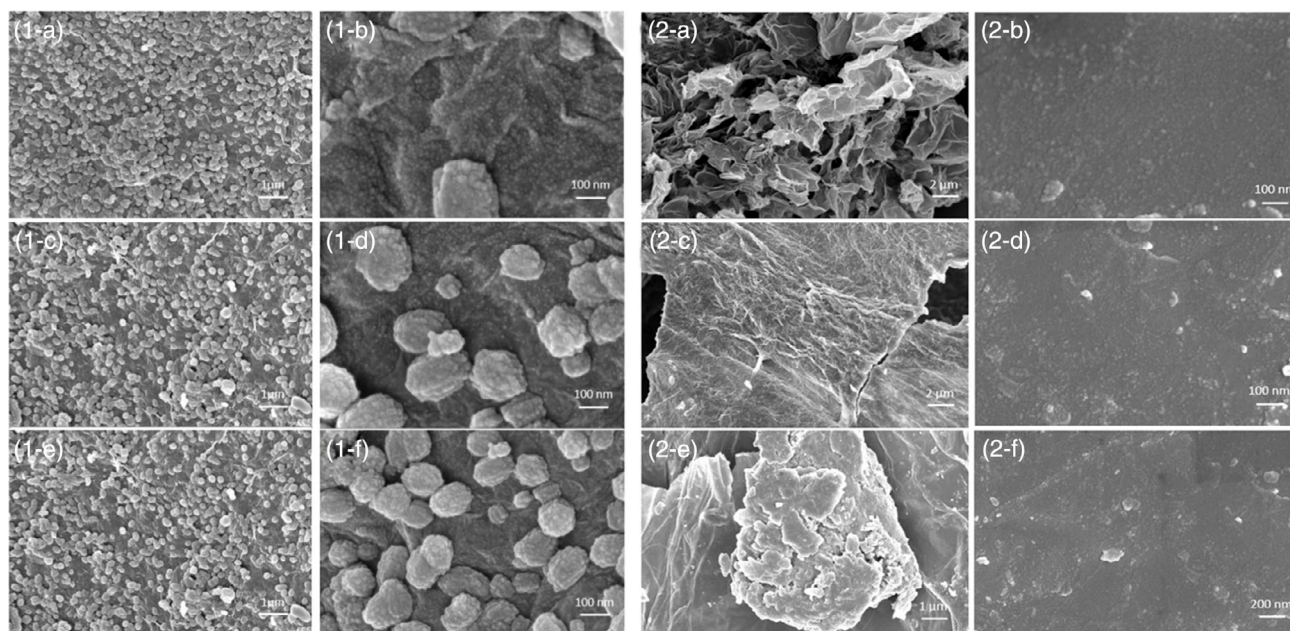


Figure 5. SEM images of: 1-a,b) 3D-GF-PA-LiOH·H₂O-37%, 1-c,d) 3D-GF-PA-LiOH·H₂O-51%, 1-e,f) 3D-GF-PA-LiOH·H₂O-70%, 2-a,b) 3D-GF-AA-LiOH·H₂O-23%, 2-c,d) 3D-GF-AA-LiOH·H₂O-51%, 2-e,f) 3D-GF-AA-LiOH·H₂O-68%.

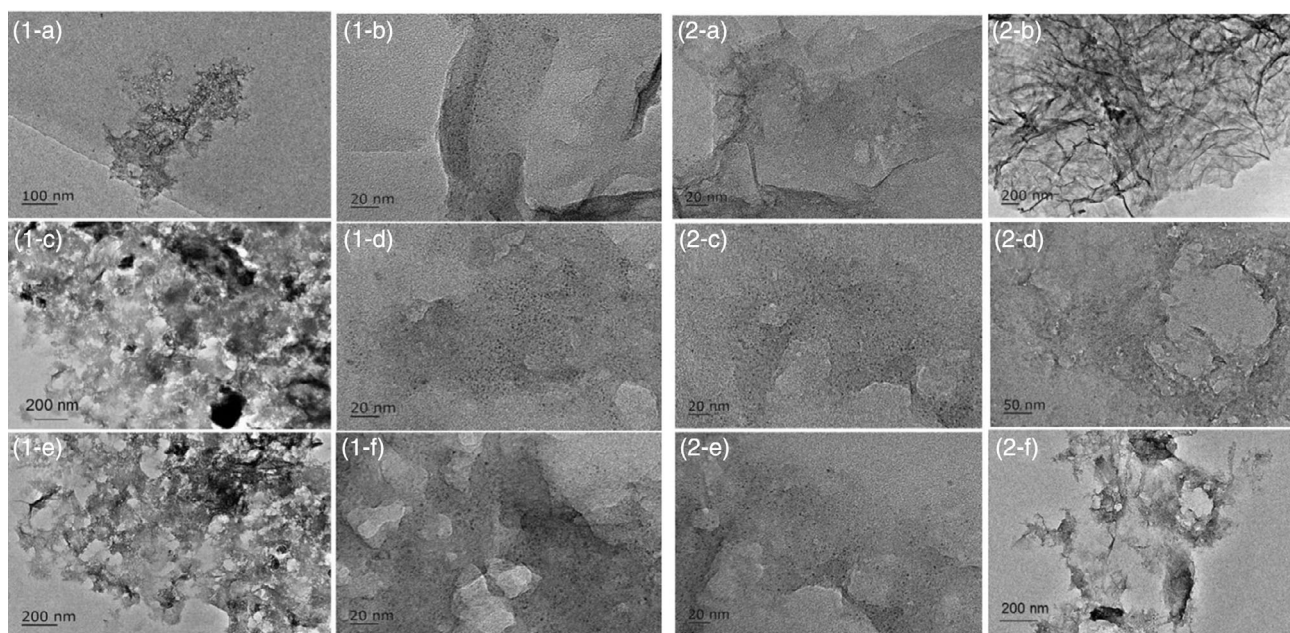


Figure 6. TEM images of: 1-a,b) 3D-GF-PA-LiOH·H₂O-37%, c,d) 3D-GF-PA-LiOH·H₂O-51%, 1-e,f) 3D-GF-PA-LiOH·H₂O-70%, 2-a,b) 3D-GF-AA-LiOH·H₂O-23%, 2-c,d) 3D-GF-AA-LiOH·H₂O-51%, 2-e,f) 3D-GF-AA-LiOH·H₂O-68% composites.

LiOH·H₂O, lessens the particle size, resulting in facilitating more contact with water molecules in the hydration process that improves the hydration rate. Third, when the 3D-GF is combined with LiOH·H₂O, the particle size of LiOH·H₂O will reach nano-scale, contributing to a pronounced increase in the number of surface atoms; moreover, the crystal field and binding energy of the internal atoms are significantly different from those of the surface atoms, which have many dangling bonds due to

the lack of adjacent atoms, leading to the enhancement of nanoparticles' thermodynamic properties.^[50,51]

3D Graphene materials have noncovalent and covalent functionalization. Covalent functionalization of 3D graphene materials mainly has two ways: 1) the covalent linkage between unsaturated C=C bonds of graphene and free radicals or dienophiles and 2) the covalent linkage between oxygen-containing groups of graphene and organic functional groups on

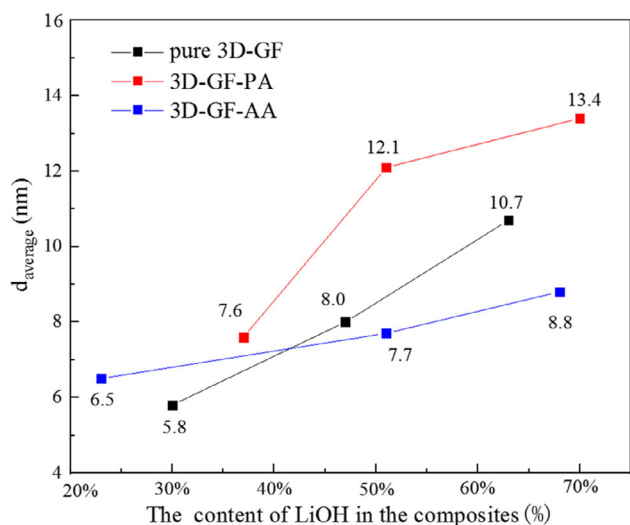


Figure 7. Average diameter of $\text{LiOH}\cdot\text{H}_2\text{O}$ particles in the composites modified by none, PA and AA.

Table 1. Texture parameters of $\text{LiOH}\cdot\text{H}_2\text{O}$ and 3D-GF- $\text{LiOH}\cdot\text{H}_2\text{O}$ composites with different additives.

Samples	The highest BET surface area [$\text{m}^2 \text{g}^{-1}$]	Average pore size [nm]
$\text{LiOH}\cdot\text{H}_2\text{O}$	15	45
3D-GF- $\text{LiOH}\cdot\text{H}_2\text{O}$	100	4
3D-GF-PA- $\text{LiOH}\cdot\text{H}_2\text{O}$	68	4
3D-GF-AA- $\text{LiOH}\cdot\text{H}_2\text{O}$	119	4

functionalization agent.^[68,69] These composites mainly focuses on enhancing the covalent functionalization and weakening the hydrophobic attraction depending on the π structure and functional groups on graphene materials.^[70] So the 3D-GF-PA and 3D-GF-AA have stronger binding ability with structural $-\text{OH}$. As AA molecules are smaller and more hydrophilic, it is more conducive to hydration.

In comparison with the pure $\text{LiOH}\cdot\text{H}_2\text{O}$, the addition of PA or AA can both broaden the charging temperature range from 60–110 to 30–200 °C that will markedly expand the scope of

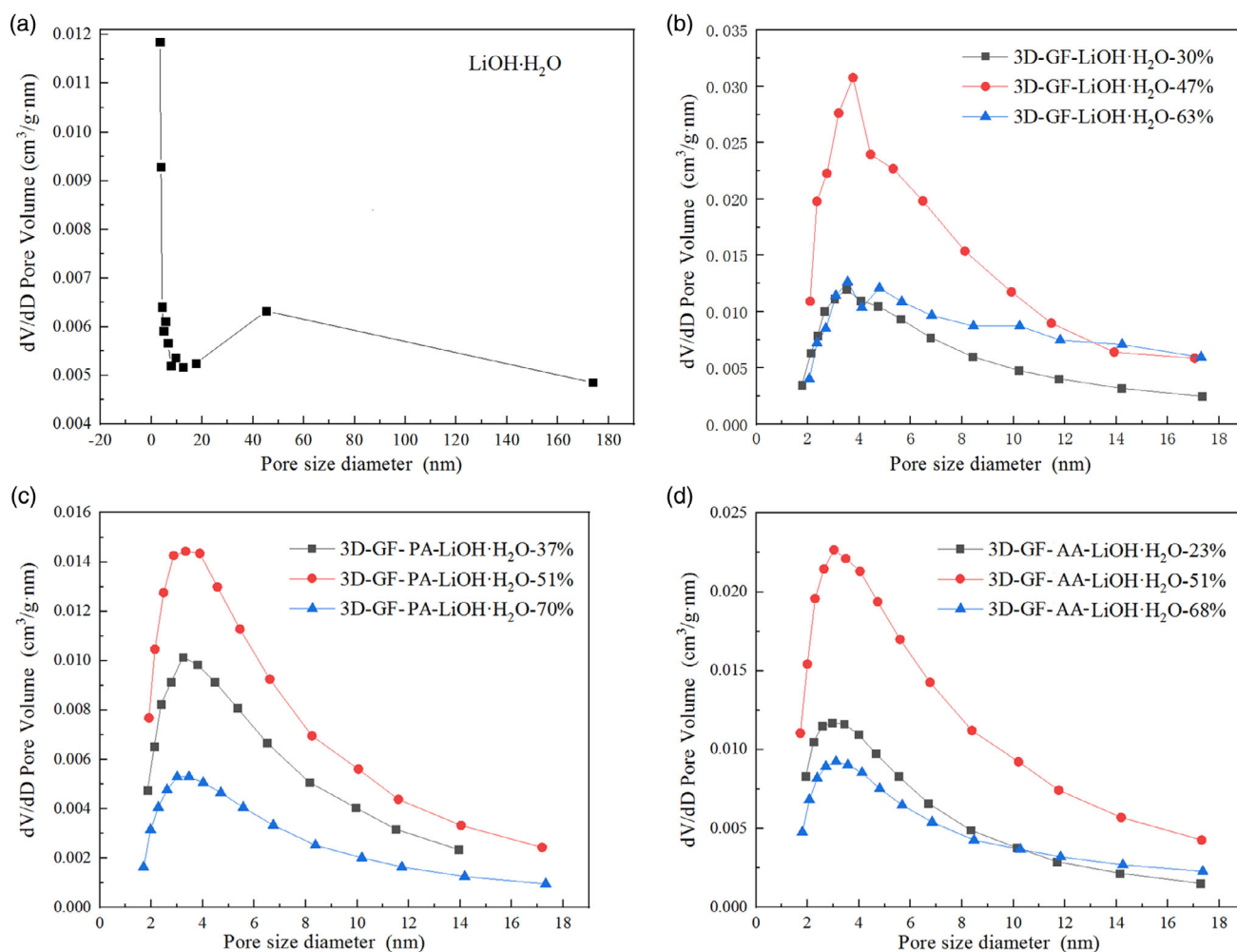


Figure 8. Pore size distribution of: a) $\text{LiOH}\cdot\text{H}_2\text{O}$; b) 3D-GF- $\text{LiOH}\cdot\text{H}_2\text{O}$; c) 3D-GF-PA- $\text{LiOH}\cdot\text{H}_2\text{O}$; and d) 3D-GF-AA- $\text{LiOH}\cdot\text{H}_2\text{O}$.

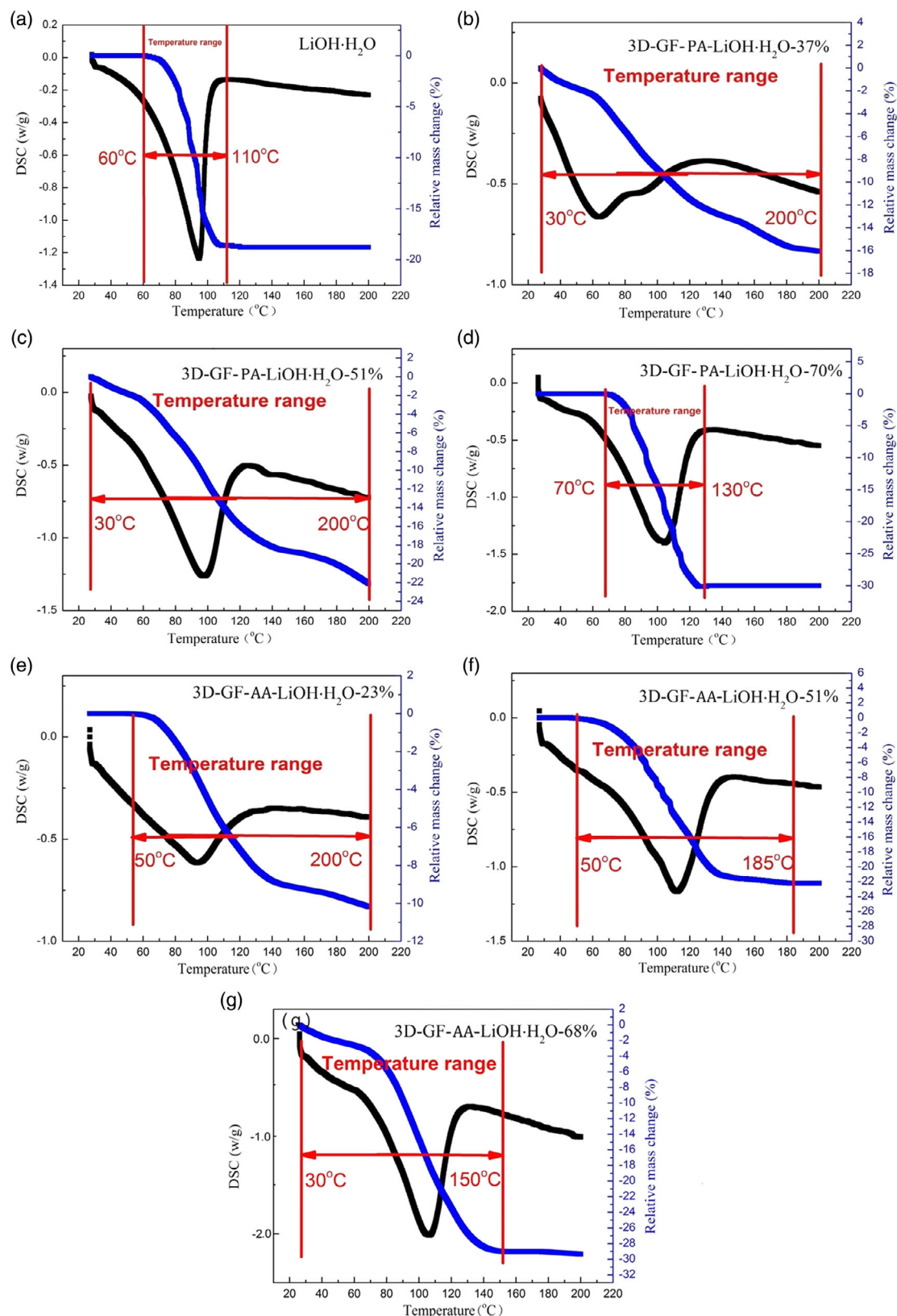


Figure 9. TG-DSC curves of a) LiOH·H₂O, b-d) 3D-GF-PA-LiOH·H₂O, and e-g) D-GF-AA-LiOH·H₂O (blue line: TG curve, black line: DSC curve).

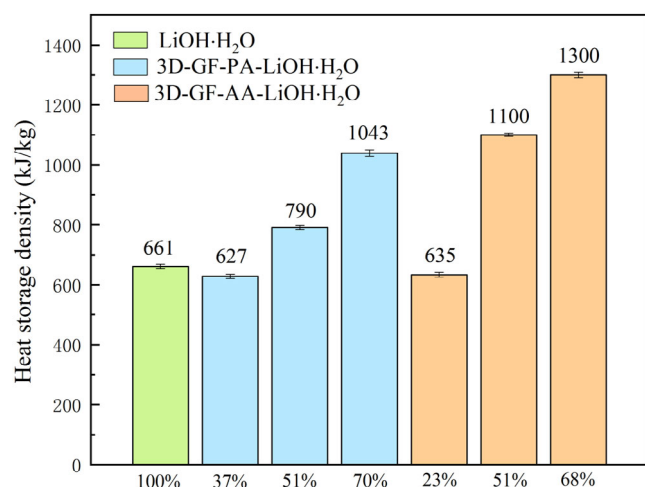


Figure 10. Heat storage density of LiOH·H₂O, 3D-GF-PA-LiOH·H₂O, and 3D-GF-AA-LiOH·H₂O.

utilizable heat energy and effectively improve the energy utilization rate, as shown in Figure 9. Moreover, the increase in heat storage density of the composites modified by AA is more notable than that of the composites modified by PA. Accordingly, we can conclude that AA is more conducive to improving the composite's heat storage density.

As shown in Figure 11, the modified composites show higher thermal conductivity than that of pure LiOH·H₂O due to the excellent thermal conductivity of modified 3D-GF who possesses 3D carbon skeleton structure providing an outstanding 3D heat conduction network for LiOH·H₂O. It is noticed that the modified composite's thermal conductivity is apt to decrease when the LiOH content in composite increases, due to the reduction of composite's structural order induced by the combination of LiOH. In addition, the thermal conductivity of the 3D-GF-AA-LiOH·H₂O composites decreases more gently with increasing LiOH content than that of 3D-GF-PA-LiOH·H₂O composites. Because AA is smaller, more uniform and easier to enter the

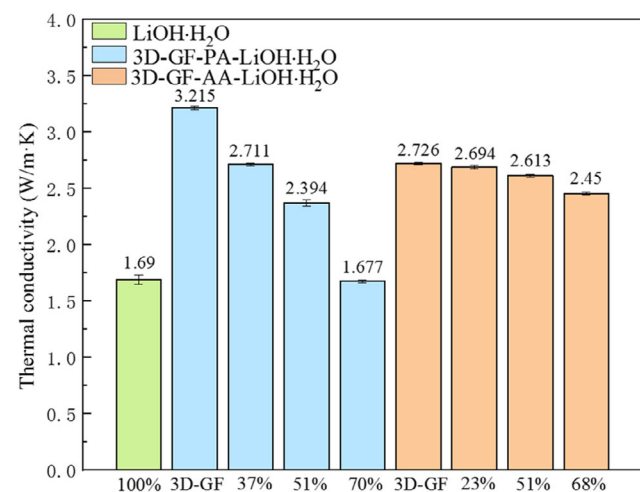


Figure 11. Variation in thermal conductivity of LiOH·H₂O, 3D-GF-PA-LiOH·H₂O, and 3D-GF-AA-LiOH·H₂O.

carbon channel, the internal heat transfer of 3D-GF-AA-LiOH·H₂O is more uniform.^[71,72] The thermal conductivity standard deviation of 3D-GF-AA-LiOH·H₂O is 0.123 which is less than that of 3D-GF-PA-LiOH·H₂O (0.644). It indicates that AA is a more suitable additive for the high loading content of LiOH than PA, which makes the composites have larger heat storage density and higher thermal conductivity.

3. Conclusions

This study focused on developing novel TCMs to obtain high heat energy density and thermal conductivity for low-grade heat storage using LiOH and 3D-GF modified with PA or AA. The influences of additives concentration on the morphology and thermal conductivity of 3D-GF were first evaluated. Subsequently, the morphology, microstructure, specific surface area, thermal conductivity, and heat storage performance of novel composite materials with different LiOH contents were experimentally investigated and discussed. The main conclusions were summarized as follow: 1) With the increase in additive concentration, the thermal conductivity of both modified 3D-GF materials first increase and reach their maximum values at 8 mg mL⁻¹, and then decrease. The 3D-GF materials retain their original structure after modified by the additives. 2) In comparison with 3D-GF-PA, 3D-GF-AA is more conducive to increasing the specific surface area of composite, enhancing the dispersity of nano-sized LiOH·H₂O particles, and lowering the particle size. 3) The addition of 3D-GF-PA and 3D-GF-AA can broaden the charging temperature range from 60–110 to 30–200 °C and improve the LiOH hydration rate and heat storage density. Compared with the 3D-GF-PA-LiOH·H₂O, 3D-GF-AA-LiOH·H₂O shows higher heat storage density with the highest value of 2763 kJ kg⁻¹–LiOH·H₂O, which is 4.2 times of pure LiOH·H₂O. 4) The modified composite's thermal conductivity is apt to decrease when the LiOH content in composite increases but is still reasonable to allow the practical application. Results indicate that AA is less affected by the LiOH content change compared with PA, which makes the composites have larger heat storage density and higher thermal conductivity.

Based on the aforementioned results, the composite modified with AA proves to be a promising TCMs suitable for low-grade heat storage with the help of high heat storage density and thermal conductivity. Further research will investigate the system performance using the modified composite material in real operating conditions.

4. Experimental Section

Materials and Preparation Procedure: All raw materials used were purchased from Aladdin, Ltd. The preparation of 3D-GF includes two steps: 1) the preparation of graphite oxide (GO), which is used as the precursor for 3D-GF by Hummers method, and 2) the synthesis of 3D-GF by hydrothermal method. First, a certain amount of sodium nitrate and 98% concentrated sulfuric acid was added into a beaker placed in the ice water bath, followed by the addition of natural flake graphite. Simultaneously, a certain amount of potassium permanganate was slowly added into the above solution, and then the solution was gradually raised to 40 °C. An hour later, the solution was diluted with distilled water and left for 30 min before heated up to 80 °C. Next, 30% of hydrogen peroxide was

added, and finally, the solution was cooled at room temperature to obtain graphite oxide. The GO was washed several times with 5% HCl and then washed to neutral with distilled water. The GO was on dialysis for 1 week, during which the distilled water was changed every 6 h. After dialysis, the GO dispersing solution was exfoliated by the ultrasonic using graphite oxide and deionized water in an ultrasonic cleaner. Then, a specific concentration of PA (or AA) solution was mixed with the obtained GO and used with the ultraviscoson at room temperature for 20–60 min. Subsequently, the mixture was dialyzed in deionized water for 10–24 h. Next, the obtained mixture was transferred into a 150 mL hydrothermal reactor, reacted at different conditions, and then naturally cooled to room temperature. Finally, the obtained product was freeze-dried at -40°C for 24 h to obtain PA (or AA)-modified 3D-GF. For convenience, the PA-modified 3D-GF and AA-modified 3D-GF were referred to as 3D-GF-PA and 3D-GF-AA, respectively.

The 3D-GF-LiOH-H₂O composite TCMs were also prepared by the hydrothermal method. First, the LiOH solution was mixed with 3D-GF-PA (or 3D-GF-AA) in different proportions and then added into the 150 mL high-pressure reactor. Next, the reactor was heated to 105°C for 12 h, and then the reactor was naturally cooled to room temperature. After that, the composites were taken out to be freeze dried, and then the final composites were put into a tubular furnace and hydrolyzed at 150°C for 3 h in an argon atmosphere. After hydrolysis, the materials were cooled down to 30°C and then hydrated at the water vapor partial pressure of 2.97 kPa with nitrogen as carrier gas at 30°C . Composite 3D-GF-LiOH-H₂O TCMs with different LiOH-H₂O content were obtained after hydration reaction. All the composites were prepared with the same path and denoted as 3D-GF-PA-LiOH-H₂O-n and 3D-GF-AA-LiOH-H₂O-n for PA-modified composite and AA-modified composite, respectively (n represents the LiOH-H₂O content).

Characterization Methods: The surface morphology and microstructure were investigated by the cold-field SEM (S-4800, Hitachi Limited) and the TEM equipped with a FEI Tecnai G212 operated at 100 kV and a JEOL JEM-2100F controlled at 200 kV. The crystal structures of the samples were analyzed by XRD performed on D8-advance X-ray diffractometer (German Bruker) using Cu target (40 kV, 40 mA) with the scanning step of 0.0167° and counting time of 10.160 s. The thermal conductivity of the samples was evaluated by the heat flow meter method (DRL-II, Xiangtan Xiangyi Instrument co., Ltd.). The BET surface area and pore characteristic were quantified by the nitrogen physical adsorption method with relative pressure of 0.1–1.0 (Quantachrome QDS-30 analyzer).

After obtaining hydrated composite materials, the samples' heat storage density and dehydration temperature were measured with the TG-DSC (STA-200, Nanjingdazhan Co., Ltd.), which was also used for measuring weight change during the dehydration step at the same time. The TG-DSC curves were obtained by heating the samples from 30°C to 200°C at the heating rate of 10 K min^{-1} under a nitrogen atmosphere.

Acknowledgements

The authors gratefully acknowledge financial support from Key Research Program of Frontier Sciences, Chinese Academy of Sciences, China [QYZDY-SSW-JSC038], Science and Technology project of China Energy Investment Corporation [GJNY-20-121] and Science Technology Planning Project of Guangdong Province, China [2017A050501046]. At the same time, thanks for the experimental help of Juan Fu in GIEC.

Conflict of Interest

The authors declare no conflict of interest.

Data Availability Statement

The data that support the findings of this study are available from the corresponding authors upon reasonable request.

Keywords

3D graphene, ascorbic acid, lithium hydroxide monohydrate, nanoparticles, phytic acid, thermochemical storages

Received: December 10, 2020

Revised: February 21, 2021

Published online: April 14, 2021

- [1] *Profiting from low-grade heat the Watt Committee on Energy Report*, No. 26, Institution of Engineering and Technology, London **1994** Institution of Engineering and Technology.
- [2] A. Mehari, Z. Y. Xu, R. Z. Wang, *Energ. Convers. Manage.* **2020**, 206, 112482.
- [3] C. Agrafiotis, A. Becker, M. Roeb, C. Sattler, *Energy* **2016**, 139, 676.
- [4] H. S. Deshmukh, S. B. Thombre, *Desalination* **2017**, 410, 91.
- [5] Y. B. Tao, Y. L. He, *Renew. Sust. Energ. Rev.* **2018**, 93, 245.
- [6] A. Rosato, S. Sibilio, *Int. J. Refrig.-Rev. Int. Froid* **2013**, 36, 717.
- [7] C. W. Chan, J. Ling-chin, A. P. Roskilly, *Appl. Therm. Eng.* **2013**, 50, 1257.
- [8] P. Pardo, A. Deydier, Z. Anxionnaz-Minvielle, S. Rougé, M. Cabassud, P. Cognet, *Renew. Sust. Energ. Rev.* **2014**, 32, 591.
- [9] K. E. N'Tsoukpoe, F. Kuznik, *Renew. Sust. Energ. Rev.* **2021**, 139, 110683.
- [10] A. H. Abedin, M. A. Rosen, *Energy J.* **2011**, 4, 42.
- [11] K. E. N'Tsoukpoe, G. Restuccia, T. Schmidt, X. Py, *Energy* **2014**, 77, 983.
- [12] V. Mamania, A. Gutiérrez, S. Ushak, *Sol. Energy Mater. Sol. Cells* **2018**, 176, 346.
- [13] Md. P. Islam, T. Morimoto, *Renewable Sustainable Energy Rev.* **2018**, 82, 2066.
- [14] A. Sole, L. Miro, C. Barreneche, I. Martorell, L. F. Cabeza, *Renewable Energy* **2015**, 75, 519.
- [15] T. Yan, R. Z. Wang, T. X. Li, L. W. Wang, I. T. Fred, *Renewable Sustainable Energy Rev.* **2015**, 43, 13.
- [16] J. Lin, Q. Zhao, H. Huang, H. Mao, Y. Liu, Y. Xiao, *Sol Energy* **2021**, 214, 149.
- [17] N. Yu, R. Z. Wang, Z. S. Lu, L. W. Wang, *Chem. Eng. Sci.* **2014**, 111, 73.
- [18] B. Dawoud, U. Vedder, E.-H. Amer, S. Dunne, *Int. J. Heat Mass Transf.* **2007**, 50, 2190.
- [19] J. S. Kharbanda, S. K. Yadav, V. Sonl, A. Kumar, *J. Energy Storage* **2020**, 31, 101712.
- [20] J. Stengler, I. Bürger, M. Linder, *Int. J. Heat Mass Transf.* **2021**, 167, 120797.
- [21] S. Wu, T. X. Li, T. Yan, R. Z. Wang, *Energy* **2019**, 175, 1222.
- [22] D. Müller, C. Knoll, G. Gravogl, C. Jordan, E. Eitenberger, G. Friedbacher, W. Artner, J. M. Welch, A. Werner, M. Harasek, R. Miletich, P. Weinberger, *Appl. Energy* **2021**, 285, 116470.
- [23] T. Yana, C. Y. Wang, D. Li, *Appl. Therm. Eng.* **2019**, 150, 512.
- [24] T. Yan, R. Z. Wang, T. X. Li, *Energy* **2018**, 143, 562.
- [25] J. Fitó, A. Coronas, S. Mauran, N. Mazeta, M. Perier-Muzeta, D. Stitou, *Energy Conv. Manage.* **2019**, 180, 709.
- [26] A. Grekova, S. Strelva, L. Gordeeva, Y. Aristov, *Energy* **2019**, 186, 115775.
- [27] L. G. Gordeeva, Y. I. Aristov, *Energy* **2011**, 36, 1273.
- [28] L. Calabrese, V. Brancato, V. Paolomba, E. Proverbio, *Renewable Energy* **2019**, 138, 1018.
- [29] Y. Zhao, C. Y. Zhao, C. N. Markides, H. Wang, W. Li, *Appl. Energy* **2020**, 280, 115950.
- [30] G. Wanga, C. Xua, G. Wei, X. Du, *Energy Procedia* **2019**, 158, 4423.
- [31] S. Li, H. Huang, X. Yang, Y. Bai, J. Li, N. Kobayashi, M. Kubota, *Appl. Therm. Eng.* **2018**, 128, 706.

- [32] M. Kubota, S. Matsumoto, *Appl. Therm. Eng.* **2019**, 150, 858.
- [33] X. Yang, H. Huang, Z. Wang, M. Kubota, Z. He, N. Kobayashi, *Chem. Phys. Lett.* **2016**, 644, 31.
- [34] X. Yang, S. Li, H. Huang, J. Li, N. Kobayashi, M. Kubota, *Energies* **2017**, 10, 644.
- [35] M. Kubota, S. Matsumoto, H. Matsuda, H. Huang, Z. He, X. Yang, *Adv. Mater. Res.* **2014**, 953–954, 757.
- [36] W. Li, J. J. Klemeš, Q. Wang, M. Zeng, *J. Clean. Prod.* **2021**, 285, 124907.
- [37] S. Salviati, F. Carosio, F. Cantamessa, L. Medina, L. A. Berglund, G. Saracco, A. Fina, *Renewable Energy* **2020**, 160, 698.
- [38] S. Li, H. Huang, X. Yang, C. Wang, N. Kobayashi, M. Kubota, *Nanoscale Microscale Thermophys. Eng.* **2017**, 21, 1.
- [39] S. Li, H. Huang, J. Li, N. Kobayashi, Y. Osaka, Z. He, H. Yuan, *RSC Adv.* **2018**, 16, 48.
- [40] Z. Sun, S. Fang, Y. H. Hu, *Chem. Rev.* **2020**, 120, 10336.
- [41] M. S. Mauter, M. Elimelech, *Environ. Sci. Technol.* **2008**, 42, 5843.
- [42] S. Nardecchia, D. Carriazo, M. L. Ferrer, M. C. Gutiérrez, F. Del Monte, *Chem. Soc. Rev.* **2013**, 42, 794.
- [43] J. Bai, Y. Li, P. Jin, J. Wang, L. Liu, *J. Alloys Compd.* **2017**, 729, 809.
- [44] B. H. Cho, W. B. Ko, *J. Nanosci. Nanotechnol.* **2013**, 13, 7625.
- [45] S. Han, D. Wu, S. Li, F. Zhang, X. Feng, *Adv. Mater.* **2014**, 26, 849.
- [46] V. H. Luan, H. N. Tien, S. H. Hur, *J. Colloid Interface Sci.* **2015**, 437, 181.
- [47] C. Lee, X. Wei, J. W. Kysar, J. Hone, *Science* **2008**, 321, 385.
- [48] S. Sun, P. Wu, *J. Mater. Chem.* **2011**, 21, 4095.
- [49] Y. Chen, P. Xu, Z. Shu, M. Wu, L. Wang, S. Zhang, Y. Zheng, H. Chen, J. Wang, Y. Li, J. Shi, *Adv. Funct. Mater.* **2014**, 24, 4386.
- [50] H. Liu, H. Qi, *Chem. Eng. J.* **2020**, 393, 124691.
- [51] B. Y. Z. Hiewa, L. Y. Lee, X. J. Lee, S. Thangalazhy-Gopakumara, S. Gan, S. S. Lim, G.-T. Pan, T. C.-K. Yang, W. S. Chiuc, P. S. Khiew, *Process Saf. Environ. Protect.* **2018**, 116, 262.
- [52] Y. Wu, J. Zhu, L. Huang, *Carbon* **2019**, 143, 610.
- [53] J. Yang, G.-Q. Qi, Y. Liu, R.-Y. Bao, Z.-Y. Liu, W. Yang, B.-H. Xie, M.-B. Yang, *Carbon* **2016**, 100, 693.
- [54] G. Qi, J. Yang, R. Bao, D. Xia, M. Cao, W. Yang, M. Yang, D. Wei, *Nano Res.* **2017**, 10, 802.
- [55] L. Zhang, R. Li, B. Tang, P. Wang, *Nanoscale* **2016**, 8, 14600.
- [56] H. A. Ousaleh, S. Sair, S. Mansouri, Y. Abboud, A. Faik, A. E. Bouari, *Sol. Energy Mater. Sol. Cells* **2020**, 215, 110601.
- [57] S. J. Li, Degree Thesis, University of Chinese Academy of Sciences, **2018**.
- [58] W. W. Tian, D. K. Cheng, S. Wang, C. X. Xiong, Q. L. Yang, *Appl. Surf. Sci.* **2019**, 495, 143589.
- [59] S. R. Sun, Y. Tang, C. Wu, C. D. Wan, *Anal. Chim. Acta* **2020**, 1107, 55.
- [60] C. Cheng, H. Liu, P. Dai, X. Shen, J. Zhang, T. Zhao, Z. Zhu, *J. Taiwan. Inst. Chem. E.* **2016**, 67, 532.
- [61] K. Kanishka, H. D. Silva, H. H. Huang, M. Yoshimura, *Appl. Surf. Sci.* **2018**, 447, 338.
- [62] C. Qiu, H. Chen, H. Liu, Z. Zhai, J. Qin, Y. Lv, Z. Gao, Y. Song, *Int. J. Hydrog. Energy* **2018**, 43, 21908.
- [63] Y. Shi, G. Liu, L. Wang, H. Zhang, *J. Colloid Interface Sci.* **2019**, 557, 336.
- [64] H. Wang, Y. Huang, C. Huang, X. Wang, K. Wang, H. Chen, S. Liu, Y. Wu, K. Xu, W. Li, *Electrochim. Acta* **2019**, 313, 423.
- [65] X. Zhuang, Y. Zhang, L. He, Y. Zhu, Q. Shi, Q. Wang, G. Song, X. Yan, L. Li, *J. Alloys Compd.* **2018**, 731, 1.
- [66] K. K. H. De Silva, H. H. Huang, R. K. Joshi, M. Yoshimura, *Carbon* **2017**, 119, 190.
- [67] K. Z. Brainina, N. Y. Stozhko, M. A. Bukharinova, L. G. Galperin, M. B. Vidrevich, A. M. Murzakaev, *J. Solid. State. Electrochem.* **2016**, 20, 2323.
- [68] J. Y. Kim, J. C. Grossman, *Nano Lett.* **2015**, 15, 2830.
- [69] A. Sinitskii, A. Dimiev, D. A. Corley, A. A. Fursina, D. V. Kosynkin, J. M. Tour, *ACS Nano* **2010**, 4, 1949.
- [70] Y. Lin, Y. Tian, H. Sun, T. Hagio, *Chemosphere* **2021**, 270, 129420.
- [71] B. X. Wang, L. P. Zhou, X. F. Peng, *Int. J. Thermophys.* **2006**, 27, 139.
- [72] L. J. Chen, R. Q. Zou, W. Xia, Z. P. Liu, Y. Y. Shang, J. L. Zhu, Y. X. Wang, J. H. Lin, D. G. Xia, A. Y. Cao, *ACS Nano* **2012**, 6, 10884.